

LADDER: Revisiting the Cosmic Distance Ladder with Deep Learning Approaches and Exploring its Applications

RAHUL SHAH ^{1,*}, SOUMADEEP SAHA ^{2,*}, PURBA MUKHERJEE ^{1,*}, UTPAL GARAIN ² AND SUPRATIK PAL ¹

¹*Physics and Applied Mathematics Unit
Indian Statistical Institute*

203, B.T. Road, Kolkata 700 108, India

²*Computer Vision and Pattern Recognition Unit
Indian Statistical Institute*

203, B.T. Road, Kolkata 700 108, India

ABSTRACT

We investigate the prospect of reconstructing the “cosmic distance ladder” of the Universe using a novel deep learning framework called LADDER - Learning Algorithm for Deep Distance Estimation and Reconstruction. LADDER is trained on the apparent magnitude data from the Pantheon Type Ia supernovae compilation, incorporating the full covariance information among data points, to produce predictions along with corresponding errors. After employing several validation tests with a number of deep learning models, we pick LADDER as the best performing one. We then demonstrate applications of our method in the cosmological context, including serving as a model-independent tool for consistency checks for other datasets like baryon acoustic oscillations, calibration of high-redshift datasets such as gamma ray bursts, and use as a model-independent mock catalog generator for future probes. Our analysis advocates for careful consideration of machine learning techniques applied to cosmological contexts.

Keywords: Cosmology (343) — Neural networks (1933) — Stellar distance (1595) — Type Ia supernovae (1728) — Calibration (2179) — Baryon acoustic oscillations (138) — Cosmological parameters (339)

1. INTRODUCTION

Knowledge of accurate distances to astronomical entities at various redshifts is essential for deducing the expansion history of the Universe. Observationally, however, this task is not simple since there does not exist one single standardizable measure of distances at all scales of cosmological interest. Hence one has to resort to a progressive method of calibrating distances, called the “cosmic distance ladder” method, using overlapping regions of potentially different standardizable objects as “rungs of the ladder”. The conventional distance ladder method (Riess & Breuval 2023) starts with direct measures of geometric distance measures and progresses to calibrating Cepheid variables (Freedman & Madore 2023) or Tip of the Red Giant Branch (TRGB) stars (Freedman et al. 2020), and finally Type Ia supernovae (SNIa). Conversely, the “inverse” distance ladder begins with cosmology dependent constraints on the sound horizon at drag epoch from the Cosmic Microwave Background (CMB), which is then used to calibrate distances to Baryon Acoustic Oscillations (BAO) and ultimately to SNIa at lower redshifts (Cuesta et al. 2015; Camarena & Marra 2020). SNIa are the preferred endpoints for both ladders given their property of being reliable standard candles over a wide redshift range.

A physical theory describing the expansion history of a spatially flat, homogeneous and isotropic universe is given by a cosmological model, which is assumed to be valid over the entire range of observed scales, i.e., from the present epoch ($z = 0$) to the epoch of recombination ($z_{\text{CMB}} \sim 1100$), with the Λ Cold Dark Matter (Λ CDM) model being the current standard, having six free parameters to be fixed by observations. For a Friedmann-Lemaître-Robertson-Walker universe, the cosmic distance-duality relation $d_L = (1+z)^2 d_A$ enables switching between luminosity distance d_L and angular diameter distance d_A - the two primary measures of distance in cosmology. The luminosity distances are related to this physical model as $d_L = \frac{c(1+z)}{H_0} \int_0^z \frac{dx}{E(x)}$, where,

Corresponding author: Supratik Pal
supratik@isical.ac.in

* Equal contribution.

$E(z) = H(z)/H_0$ is the reduced Hubble parameter, and $H_0 = H(z = 0)$ is the Hubble constant, signifying the rate of the Universe's expansion today. For sufficiently low redshifts, d_L is well approximated by Hubble's Law, $z = H_0 d_L/c$, offering a means to obtain H_0 without assuming a cosmological model. However, of late, inconsistencies have arisen in the concordance model, with the most significant being the tension in the measurement of the Hubble constant (H_0) (Novosyadlyj et al. 2014; Hazra et al. 2015; Bernal et al. 2016). This, and other growing issues with Λ CDM, has prompted the community to turn either to more complicated cosmological models or to cosmological model-independent (henceforth referred to as simply "model-independent") approaches, the second route proving more effective with time.

The simplest method involves cosmography (Visser 2005), which being merely a Taylor expansion of the scale factor does not introduce bias towards any particular cosmological model. There is, however, an ambiguity as to the number of terms to consider in such a series. The aforementioned issues in contemporary cosmology, such as the emergence of tensions, arise when subjected to precision data from observations. This necessitates any alternative method of building the distance ladder to maintain, if not improve, the precision of the data being used. Premature truncation of the cosmographic series may induce significant numerical errors at higher redshifts, while considering higher-order terms raises doubts on convergence. Although alternatives to the Taylor series, such as Padé (Wei et al. 2014) and Chebyshev (Capozziello et al. 2018), help overcome convergence issues to some extent, there still is no clear consensus on the exact number of terms to consider to faithfully mimic the underlying cosmology.

This has motivated the community to resort to reverse engineering by employing model-independent methods for reconstructing distances, and estimation of cosmological parameters therefrom. There have been multiple attempts to reconstruct cosmic distances using Gaussian processes (GP) and genetic algorithms (GA), by various authors, both with present and simulated data from future observatories (Keeley et al. 2021; Mukherjee & Mukherjee 2021; Arjona et al. 2021; Li et al. 2024). Ambiguity over the choice of kernels, the function dictionary, the mean function, and overfitting concerns with overwhelming errors in data-scarce regions have significantly limited the prospects of these approaches (Ó Colgáin & Sheikh-Jabbari 2021; Hwang et al. 2023). This has led to an active use of deep learning with artificial neural networks (ANN) (Wang et al. 2020b; Escamilla-Rivera et al. 2022; Olvera et al. 2022; Gómez-Vargas et al. 2023a,b; Giambagli et al. 2023; Dialektopoulos et al. 2023, 2024; Mukherjee et al. 2024a; Zhang et al. 2023, 2024; Xie et al. 2023; Tang et al. 2021; Wang et al. 2020a; Mehrabi 2023; Liu et al. 2023) in this domain.

As important accuracy is, measuring distances is limited by experimental precision, due to astrophysical uncertainties, foregrounds, peculiar velocity effects and other practical limitations. Precision is also limited by the available number of data points. These are a critical concern as precision tests are essential for scrutinizing the standard, or alternative, cosmological models. Although both these issues are hoped to be improved upon considerably by upcoming observatories, the use of innovative analysis methods *viz.* Machine Learning (ML) techniques on current data could help overcome these challenges. Another common limitation for a majority of previous ML attempts in cosmology is in the correct and stable prediction of errors at relatively higher redshifts, which makes them unsuitable for undertaking precision cosmological tests when it comes to the issue of tensions. With this motivation, we present our approach - LADDER - Learning Algorithm for Deep Distance Estimation and Reconstruction, which has been designed from the ground up keeping the above considerations in mind. Moreover, almost every straightforward technique fails at extrapolation to any redshift beyond the range of available data in a model-independent manner, due to prediction uncertainties playing the dominant role. Being able to extrapolate beyond the range of available data is lucrative since it could allow simulations of intermediate-redshift data, or in the least, serve as some stable augmentation of currently available data to higher redshifts.

In this spirit, we aim to revisit the cosmic distance ladder by presenting this novel deep learning algorithm LADDER which is trained using the Pantheon SNIa dataset (Scolnic et al. 2018), taking into account the corresponding errors and complete covariances in the data. Our algorithm interpolates from the joint distribution of a randomly chosen subset of the dataset to estimate the target variable and errors simultaneously, and elegantly incorporates correlations and the sequential nature of the data. This leads to predictions that are robust to input noise and outliers and helps make precise predictions even in data-sparse regions. In the following sections, we first outline the datasets and the proposed algorithm, followed by performance validation. We then point out a few cosmological applications that can be explored further using our algorithm. In particular, we demonstrate LADDER's versatility in conducting consistency checks for a similar SNIa dataset, Pantheon+ (Scolnic et al. 2022). Subsequently, we analyze the implications of our model-independent predictions using the BAO dataset, with regard to their alleged dependence on fiducial cosmology (Sherwin & White 2019). We then use the LADDER predictions to calibrate the high redshift Gamma Ray Bursts (GRB) dataset to derive constraints on the Λ CDM and w CDM models. Additionally, we discuss the potential of our deep learning network as a model-independent mock data generator for cosmological studies, and some future directions.

2. TRAINING DATASET

In principle, one can utilize LADDER with any dataset. However, in this article, our primary focus is on achieving a model-independent reconstruction of the cosmological distance ladder. To accomplish this, we employ the Pantheon SNIa compilation (Scolnic et al. 2018) as our training dataset. The Pantheon dataset offers several cosmological advantages for model-independent reconstruction of the cosmic distance ladder. Firstly, it remains uncalibrated, which guarantees that it is neither plagued by the choice of cosmological models nor biased by any inherent systematics in otherwise model-independent direct distance measurement calibration methods. Moreover, it involves fewer sources of uncertainties, enhancing its robustness. Additionally, its broad redshift range and diverse data samples help ensure unbiased learning. Notably, no *a priori* priors on the calibration parameter (M_B , the absolute magnitude of SNIa in the B-band) are imposed on the ‘‘Pantheon’’ dataset during training, either from early-time model-dependent CMB constraints or direct late-time distance measurements.

Pantheon features rich data from 1048 spectroscopically confirmed SNIa spanning a broad range of redshifts $0.01 \lesssim z < 2.3$ with a higher sample density at lower redshifts, and notable sparsity with increasing z . This dataset comprises observations on direct measurement of the apparent magnitude (m) with the statistical uncertainties (Δm) tabulated at different redshifts (z). Additionally, there is a 1048×1048 matrix \mathbf{C}_{sys} corresponding to covariances among the data points. This dataset thus allows for a thorough exploration of cosmic distances covering a wide range of redshifts, and is well-suited for model-independent analyses.

Given knowledge of M_B , one can find the luminosity distance $d_L(z)$ independent of any cosmological model. This is expressed by the equation,

$$\mu(z) = 5 \log_{10} \frac{d_L(z)}{\text{Mpc}} + 25, \quad (1)$$

where $\mu(z) = m(z) - M_B$ is the distance modulus.

The observed apparent magnitudes (\tilde{m}) for each SNIa light curve as measured on Earth depends on the heliocentric (z_{hel}) and CMB frame (z_{cmb}) redshifts. In terms of only z_{cmb} (i.e. in the absence of peculiar velocities) we have,

$$m(z_{\text{cmb}}) = \tilde{m}(z_{\text{hel}}, z_{\text{cmb}}) - 5 \log_{10} \left(\frac{1 + z_{\text{hel}}}{1 + z_{\text{cmb}}} \right). \quad (2)$$

We then also propagate the errors in z_{cmb} into $m(z_{\text{cmb}})$. This gives us the data in the final form $m(z_{\text{cmb}})$ vs z_{cmb} , which we henceforth refer to as simply m vs z , with corresponding statistical errors Δm and covariance matrix \mathbf{C}_{sys} .

Armed with this data, we aim to train a neural network capable of proficiently learning, and extrapolating to higher redshifts, the apparent magnitude dataset independently of an underlying cosmological model.

3. METHODOLOGY

3.1. Formal Problem Description

Given the Pantheon dataset, $\mathcal{D} = \{(z_i, m_i, \Delta m_i) | \forall i \in \{1, \dots, N\}\}$, $z_i, m_i \in \mathbb{R}$ which is drawn from some *a priori* unknown distribution, and \mathbf{C}_{sys} , we are interested in estimating the distribution of $\mathcal{P}(M = m | z) \forall z \in \mathbb{R}^+$ with the assumption, $\mathcal{P}(M = m | z) = \mathcal{N}(\mu_\theta(z), \sigma_\theta(z))$, for some functions $\mu_\theta, \sigma_\theta$ and some parameter θ . In ML parlance this would be restated as - given $(\mathcal{D}, \mathbf{C}_{\text{sys}})$ find $f : \mathcal{Z} \rightarrow \mathbb{R}^2$, such that for any new input z , we have,

$$\min_{f \in \mathcal{F}} \mathcal{E} \left(\mathcal{N}(f(z)_1, f(z)_2) \right), \quad (3)$$

for a certain class of functions \mathcal{F} , which could be a deep learning network and \mathcal{E} is a risk functional. This risk functional is typically the empirical risk,

$$\mathcal{E}^{\text{empirical}} = \sum_{i=1}^N \ell \left(\mathcal{N}(m_i, \Delta m_i), \mathcal{N}(f(z_i)_1, f(z_i)_2) \right), \quad (4)$$

where ℓ is a loss-function, usually Kullback-Leibler (KL) divergence since we are measuring the distance between distributions.

Although our goal is to interpolate from the given points, this problem notably differs from standard regression as the samples are not independent. In particular, since $\mathcal{P}(m_1, m_2, \dots, m_N | z_1, z_2, \dots, z_N) \neq \prod_{i=1}^N \mathcal{P}(m_i | z_i)$, our typical empirical risk minimization does not work, and we are left dealing with the following intractable empirical risk,

$$\mathcal{E}^{\text{empirical}} = \ell \left(\mathcal{N}((m_1, m_2, \dots, m_N), \Sigma_m), \mathcal{N}((f(z_1)_1, f(z_2)_1, \dots, f(z_N)_1), \Sigma_f) \right). \quad (5)$$

3.2. Our Approach - LADDER

Since our data points are not independent, any predictive model we devise would have to depend on the entire dataset. This presents a challenge, as, whenever we have access to any new data, we must re-adjust our predictive model taking into account the correlations between the new and old data. In order to mitigate this issue without ignoring the correlations between the data instances, we assume that at most K many samples from the dataset are correlated with each other, and rewrite the empirical risk as,

$$\mathcal{E}^{\text{empirical}} \approx \sum_{\text{all combinations } j_1, \dots, j_K} \ell \left(\mathcal{N}((m_{j_1}, \dots, m_{j_K}), \Sigma_m^K), \mathcal{N}((f(z_{j_1})_1, \dots, f(z_{j_K})_1), \Sigma_f^K) \right), \quad (6)$$

where Σ_f^K, Σ_m^K are the predicted and observed covariances respectively, and f is our predictive model. This way, although we are not considering the whole covariance matrix Σ_m for each sample, all possible correlations are accounted for, since we are minimizing risk over all observed data-points in aggregate. This motivates our choice of function to be of the form,

$$\begin{aligned} f_\theta : \mathbb{R}^{2 \cdot K-1} &\rightarrow \mathbb{R} \times \mathbb{R}^+, \\ f_\theta(z; z_{j_1}, z_{j_2}, \dots, z_{j_{K-1}}, m_{j_1}, m_{j_2}, \dots, m_{j_{K-1}}) &\mapsto (\mu_z, \sigma_z), \\ \mathcal{N}(\mu_z, \sigma_z) &\approx \mathcal{P}(m|z; z_{j_1}, z_{j_2}, \dots, z_{j_{K-1}}, m_{j_1}, m_{j_2}, \dots, m_{j_{K-1}}). \end{aligned} \quad (7)$$

Our objective then is to minimize,

$$\begin{aligned} \mathcal{E}^{\text{empirical}} &\approx \sum_{\text{all combinations } j_1, \dots, j_K} \sum_{k=1}^N \ell \left(\mathcal{N}(m_k, \Delta m_k), \mathcal{N}(f_\theta(z_k; z_{j_1}, z_{j_2}, \dots, m_{j_{K-1}})) \right), \\ \ell(P, Q) = D_{KL}(P||Q) &= \sum_{x \in \mathcal{X}} P(x) \log \frac{P(x)}{Q(x)} \quad (\text{KL divergence}). \end{aligned} \quad (8)$$

D_{KL} is a pseudo-metric measuring the ‘‘distance’’ between the distributions P and Q . The parameter θ can be found with an algorithm like stochastic gradient descent.

During training, we first choose K points from \mathcal{D} and designate $K - 1$ as ‘‘support’’ points, and the remaining point is dubbed the ‘‘query point’’. We create a training instance by sampling from $\mathcal{N}(m_{j_2}, m_{j_3}, \dots, m_{j_K}, \Sigma_m^K)$ to get $\hat{m}_{j_2}, \hat{m}_{j_3}, \dots, \hat{m}_{j_K}$, and create $X = (z_{j_1}, z_{j_2}, \hat{m}_{j_2}, \dots, z_{j_K}, \hat{m}_{j_K})$ and $Y = (m_{j_1}, \Delta m_{j_1})$ (we rearrange the indices such that $z_{j_2} \leq z_{j_3} \leq \dots$). Put simply, the training proxy objective asks - *given these $K - 1$ points from the dataset, predict $(m, \Delta m)$ corresponding to my point of interest.*

Given j_1, j_2, \dots, j_K , we compute Σ_m^K as follows,

$$\begin{aligned} \Sigma_m &= \mathbf{C}_{\text{sys}} + \mathbb{I}_{N \times N} \cdot \left((\Delta m_1)^2, (\Delta m_2)^2, \dots, (\Delta m_N)^2 \right), \\ [\Sigma_m^K]_{\alpha, \beta} &= [\Sigma_m]_{j_\alpha, j_\beta} \quad \forall \alpha, \beta \in \{1, \dots, K - 1\}. \end{aligned} \quad (9)$$

Our job then is to find $\hat{\theta}$, such that $\hat{\theta} = \arg \min_\theta \ell[\mathcal{N}(f_\theta(X)), \mathcal{N}(m_{j_1}, \Delta m_{j_1})]$, where f_θ is a suitably chosen deep neural network, with parameters θ . The full algorithm is outlined in Algorithm 1, with a schematic outlined in Figure 1.

Our inference algorithm follows the same basic structure. Given an unseen z , we first choose $K - 1$ points from \mathcal{D} at random, and sample from $\mathcal{N}((m_{j_2}^{(i)}, \dots, m_{j_{K-1}}^{(i)}), \Sigma_m^K)$ to get $\hat{m}_{j_2}^{(i)}, \dots, \hat{m}_{j_{K-1}}^{(i)}$, and create $X_{\text{unseen}}^{(i)} = (z_{\text{unseen}}, z_{j_2}^{(i)}, \hat{m}_{j_2}^{(i)}, \dots, z_{j_{K-1}}^{(i)}, \hat{m}_{j_{K-1}}^{(i)})$. We then use $f_{\hat{\theta}}$, to compute $\mu^{(i)}, \sigma^{(i)}$. Recall, from equation (7), $\mathcal{N}(\mu_z, \sigma_z) \approx \mathcal{P}(m|z; z_{j_1}, z_{j_2}, \dots, z_{j_{K-1}}, m_{j_1}, m_{j_2}, \dots, m_{j_{K-1}})$ and we wish to model $\mathcal{P}(m|z) = \int_{z_1, \dots, z_K} \mathcal{P}(m|z; z_{j_1}, \dots, z_{j_{K-1}}, m_{j_1}, \dots, m_{j_{K-1}}) d\mu$. We approximate this with Monte Carlo,

$$\begin{aligned} \mu_{\text{predicted}}^{(i)}, \sigma_{\text{predicted}}^{(i)} &= f_{\hat{\theta}}(X_{\text{unseen}}^{(i)}), \\ \mu &= \frac{1}{P} \sum_{i=1}^P \mu_{\text{predicted}}^{(i)}, \quad \sigma = \frac{1}{P} \sum_{i=1}^P \sigma_{\text{predicted}}^{(i)}, \\ \mathcal{P}(m|z) &\approx \mathcal{N}(\mu, \sigma). \end{aligned} \quad (10)$$

In addition to being able to model correlations between data points, our approach has another key advantage. Neural networks are universal function approximators (Hornik et al. 1989) and tend to suffer from overfitting. This problem is exacerbated when dataset sizes are small, and typically we address this with regularization techniques like data augmentation, injecting perturbations

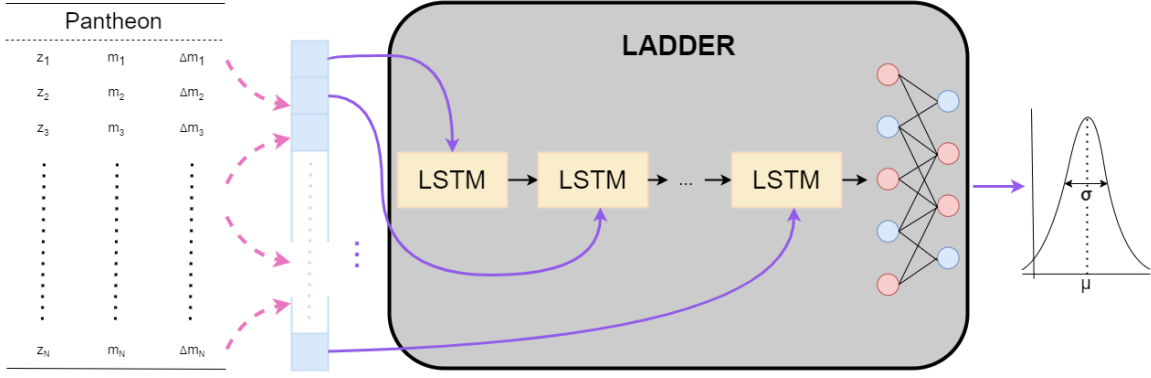


Figure 1. Schematic overview of the training algorithm.

Algorithm 1 LADDER - Learning Algorithm for Deep Distance Reconstruction and Estimation

Given \mathcal{D} , \mathbf{C}_{sys} and batch size B .

Initialize θ_0 .

while not StopCondition **do**

$l \leftarrow 0$

for $i = 1, 2, \dots, B$ **do**

 Get K samples from \mathcal{D}

$\{(z_1, m_1, \Delta m_1), \dots, (z_K, m_K, \Delta m_K)\}$

$Y_i = (m_{j_1}, \Delta m_{j_1})$

$\hat{m}_{j_2}, \hat{m}_{j_3}, \dots, \hat{m}_{j_K} \sim \mathcal{N}(m_{j_2}, m_{j_3}, \dots, m_{j_K}, \Sigma_m^K)$

 ▶ (equation (9))

$X_i = (z_{j_1}, z_{j_2}, \hat{m}_{j_2}, \dots, z_{j_K}, \hat{m}_{j_K}) \quad z_{j_2} \leq z_{j_3} \dots$

$\mu, \sigma = f_{\theta_t}(X_i)_1, f_{\theta_t}(X_i)_2$

 ▶ Forward pass.

$l += D_{KL}(\mathcal{N}(m_{j_1}, \Delta m_{j_1}), \mathcal{N}(\mu, \sigma))$

end for

 Compute $\nabla_{\theta_t} l \quad \forall \theta_t$

$\theta_{t+1} = \theta_t + \eta \cdot \nabla_{\theta_t}$

 ▶ Gradient update (illustrative).

if ... **then**

 StopCondition \leftarrow True

 ▶ Check if model converged.

end if

end while

or modifying loss functions (Zhang et al. 2017). Our approach ‘‘augments’’ data by sampling from the normal distribution defined by data points and their associated covariances, thus making outputs less sensitive to perturbations of the input. Additionally, since the neural network has to interpolate from a randomly chosen subset of data points, it cannot rely on cues from any single data point, thus making it robust to outliers. Despite random initialization, we found that models trained in this framework reliably converged to the identical final configurations, thus inspiring confidence in this approach’s ability to learn underlying causal connections.

3.3. Model architecture

We employed two popular neural network architectures for our analysis - the Multi-Layer Perceptron (MLP) (Sanger & Baljekar 1958) and Long-Short Term Memory (LSTM) networks (Hochreiter & Schmidhuber 1997).

In the multi-layer perceptron model we have $W_h \in \mathbb{R}^{n \times d}$, $b_h \in \mathbb{R}^d \forall h \in \{1, 2, \dots, H\}$, giving,

$$\begin{aligned} z_h &= \sigma(W_h \cdot z_{h-1} + b_h), \\ z_0 &= x \text{ (input)}, \\ f_{\theta}(x) &= z_H \text{ (output)}. \end{aligned} \tag{11}$$

where σ is a non-linear ‘‘transfer’’ function like sigmoid, etc. We employed a network with $H = 4$ with $W_1 \in \mathbb{R}^{2K-1 \times 16}$, $W_2, W_3 \in \mathbb{R}^{16 \times 16}$ and $W_4 \in \mathbb{R}^{16 \times 2}$.

LSTMs are a type of recurrent neural network that model a sequence of inputs x_1, x_2, \dots with intermediate representations h_t defined as,

$$h_t = f_{W_1, \dots, b_1, \dots}(x_t, h_{t-1}),$$

$$LSTM(x_1, \dots, x_T) = h_T.$$
(12)

We employed a 2-layer LSTM, with a further layer mapping $h_T \rightarrow \mathbb{R}^2$.

We additionally employed batch-normalization and dropouts as deemed appropriate and trained with the AdamW optimizer. We randomly selected 10% of the training data to serve as a validation set and used grid search to find optimal hyper-parameters. We employed a reduce learning rate on plateau strategy and early stopping using the loss on the validation set.

3.4. Performance Validation

To ensure that our proposed algorithm and network architecture are adept at learning the underlying relationship expressed in the data, we first performed some ablation studies. Since we are interested in reconstructing and extrapolating from the data, in addition to accuracy our models must demonstrate some additional cosmological properties. In particular, we expect the cosmological luminosity distance to be monotonic and smooth with respect to redshifts. Thus, we analyze the performance of our models on three metrics ¹ - mean squared error on the validation set, monotonicity as measured by Spearman correlation and smoothness, defined as,

$$\text{Smoothness}[f_\theta] = \frac{1}{n} \sum_{i=1}^n |f''_\theta(z_i)|.$$
(13)

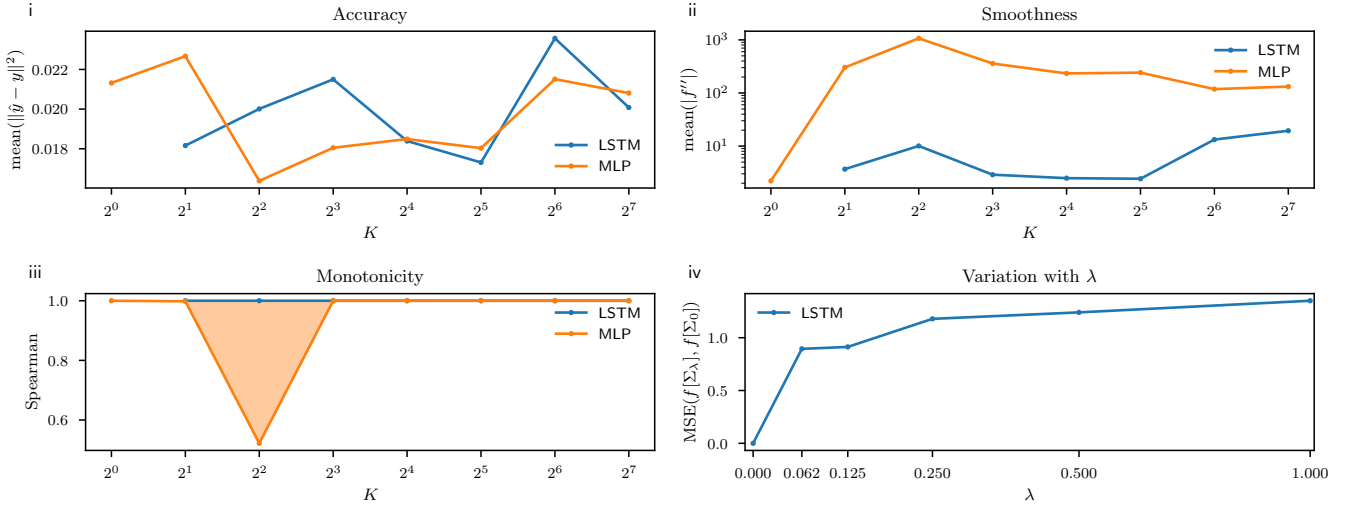


Figure 2. Results of ablation studies and validation experiments with various models. (i-iii) Variation of error, smoothness and monotonicity with K respectively. MLP models do not produce smooth, monotonic results (except $K=1$), and the $K = 1$ MLP is outperformed by the LSTM model at roughly the same smoothness and monotonicity. (iv) Prediction variation of models trained on $\Sigma|\lambda$ and Σ_0 . When the covariance matrix is progressively corrupted with noise, the predictions change, thus demonstrating our approach’s ability to model correlations.

We first studied the effect of the parameter K on the predictive performance of our models and found that the best-performing model is the LSTM with $K = 32$. In general, the MLP models were found to be lacking in smoothness, and were not reliably monotonic. We also studied how well correlations are captured by our model. To this end, we constructed,

$$\Sigma_\lambda = \lambda \mathbf{N} + (1 - \lambda) \mathbf{C}_{\text{sys}} + \mathbb{I}_{N \times N} \cdot \left((\Delta m_1)^2, (\Delta m_2)^2, \dots, (\Delta m_N)^2 \right),$$
(14)

where $\mathbf{N} = A \times A^T$; $A_{ij} \sim \mathcal{N}(0, 1)$ is a noise matrix, which is by construction symmetric and positive semi-definite. The idea is to “corrupt” the covariance matrix and study how the model predictions vary as a result (note that, $\Sigma_0 = \Sigma_m$). We measured

¹ We use a 80%-20% random split of Pantheon for this.

the distance between the distributions (D_{KL}) predicted by the model trained with Σ_λ versus those predicted by the model trained with Σ_m to see whether the predicted distributions differ. We measured D_{KL} , as the noisy covariance matrix is likely to affect the variance predictions as well. We observed that the distance between the predicted distribution of the model trained with Σ_λ and Σ_0 increases steadily with increasing λ . This shows that the model is capable of picking up cues from the correlations between data points. These results are summarized in Figure 2.

Table 1. Performance of various ML models. (\downarrow) indicates lower is better, (\uparrow) indicates higher is better.

Model	MSE (\downarrow)	Monotonicity (\uparrow)	Smoothness (\downarrow)
kNN(k=5)	0.022116	0.99999	90.67500
SVR	0.019358	1.0	3.10633
MLP(K=1)	0.022202	1.0	2.21691
MLP(K=32)	0.020484	0.99997	88.99974
LADDER	0.018495	1.0	2.30022

We also compare the performance of our model with other regression algorithms like k-Nearest Neighbor Regression (kNNR) and Support Vector Regression (SVR) as measured by accuracy, monotonicity and smoothness (see Table 1). In kNNR, we pick $k(=5)$ nearest instances from the training data and report a weighted sum of their corresponding target values. SVR is a variant of Support Vector Machines, and tries to find a function such that all training instances are within an ϵ -interval of the function. Our algorithm and architecture, outperforms other models in accuracy while maintaining monotonicity and smoothness. Our learning algorithm, outlined in Section 3.2, alongside the architecture (LSTM, K=32) is dubbed LADDER - Learning Algorithm for Deep Distance Estimation and Reconstruction. In the subsequent sections, unless explicitly stated, we report results with this approach.

4. COSMOLOGICAL APPLICATIONS OF LEARNING THE DISTANCE LADDER

Given the experimental validation of the performance of our approach in learning the distance ladder, let us now outline a few interesting cosmological applications of the algorithm, which arise as natural consequences of the training process. Of course, our intention is not to do an extensive analysis for each one, which is beyond the scope of the present article anyway. We rather intend to point out possible areas which can be explored further with LADDER, each one of them calling for detailed future investigation.

4.1. Consistency check for similar datasets in a model-independent approach

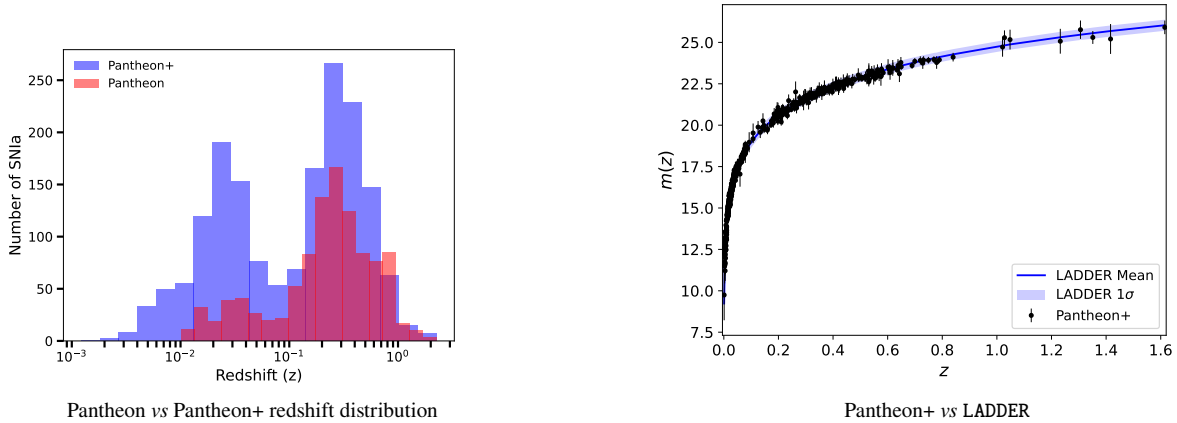


Figure 3. Testing Pantheon+ : Relative redshift distribution of the Pantheon and Pantheon+ datasets (left panel); Comparison between Pantheon-trained LADDER reconstruction vs Pantheon+ (right panel).

Having trained LADDER with Pantheon, we proceed to test the consistency of a comparable SNIa dataset in a model-independent manner. For this, we choose the Pantheon+ compilation (Scolnic et al. 2022) which is the latest publicly available SNIa dataset at the time of writing. The major reason to check consistency of Pantheon+ compilation is the following - this compilation comprises

data from 1701 light curves representing 1550 distinct SNIa over a redshift range of $0.001 \lesssim z < 2.3$. This range significantly overlaps with that of Pantheon, with a notably high data density at lower redshifts (see the left panel of Figure 3). This has potentially significant implications for our understanding of cosmic phenomena, suggesting possible variations in the underlying astrophysical or cosmological processes. This could have a notable impact on the precision of cosmological parameter estimates and the robustness of the underlying physical model, only if the extended dataset with 1701 data points are reliable enough. Several concerns regarding the Pantheon+ dataset have been raised in recent studies. For instance, [Keeley et al. \(2022\)](#) suggest that errors in the covariance matrix may have been overestimated by approximately 5%. Additionally, [Perivolaropoulos & Skara \(2023\)](#) have identified evidence of an uncorrected systematic effect, specifically volumetric redshift scatter, in the data. They also highlight a potential physical shift in the absolute magnitude of SNIa at redshift $z = 0.005$, assuming a Λ CDM background. Moreover, [Schöneberg et al. \(2022b\)](#) have reported that Pantheon+ exhibits a preference for a slightly higher value of Ω_{m0} compared to the original Pantheon dataset within the framework of Λ CDM cosmology. In the presence of such reports, and the absence of any other SNIa dataset from an independent mission, there is no way to answer directly from data as to how consistent Pantheon+ is. In this context, a well-trained and well-validated ML-based approach may act as a model-independent tool to test for such inconsistencies. Herein lies the role of LADDER.

For an unbiased assessment, we focus solely on the 753 data points in Pantheon+ which are not included in Pantheon. A comparison between these data points and the reconstructions by Pantheon-trained LADDER is presented in the right panel of Figure 3. In Figure 4 and Table 2, we show a comparison of cosmological parameter constraints obtained from the Pantheon and Pantheon+ datasets vs LADDER predictions at Pantheon+ redshifts. We see there are negligible mean shifts between Pantheon and LADDER, indicating that LADDER predictions are consistent and in good agreement with Pantheon. Moreover, having trained LADDER on Pantheon, the LADDER predictions at Pantheon+ redshifts show a generic mean shift of the cosmological parameters towards those obtained with Pantheon.

Both Pantheon and LADDER show preference for a phantom equation of state (EoS) $w < -1$. However, we find the constraints on the parameters, Ω_{m0} and w_0 , obtained from Pantheon+ have slightly changed in comparison to Pantheon (see [Schöneberg et al. \(2022b\)](#) for previous reports of such trends) or LADDER, where Pantheon+ prefers a higher value of the matter density parameter Ω_{m0} in the case of the Λ CDM model. For the w CDM model, Ω_{m0} constraint obtained from Pantheon+ is lower than that from Pantheon or LADDER. Besides, Pantheon+ data shows a preference towards a non-phantom EoS when compared with that of Pantheon or LADDER. This analysis indicates possible inconsistencies in the Pantheon+ compilation, as pointed out earlier. Nonetheless, despite these shifts, the constraints on Ω_{m0} and w obtained from the three different datasets are found to be consistent with one another at 1σ , for both the models considered. Given that the mean shifts are all within 1σ , shows the consistency of LADDER itself with the two datasets under consideration. However, in order to make any strong comments on these claims one needs to do a full MCMC analysis with LADDER predictions *vis-à-vis* Pantheon+ in combination with CMB, BAO and direct measurement datasets.

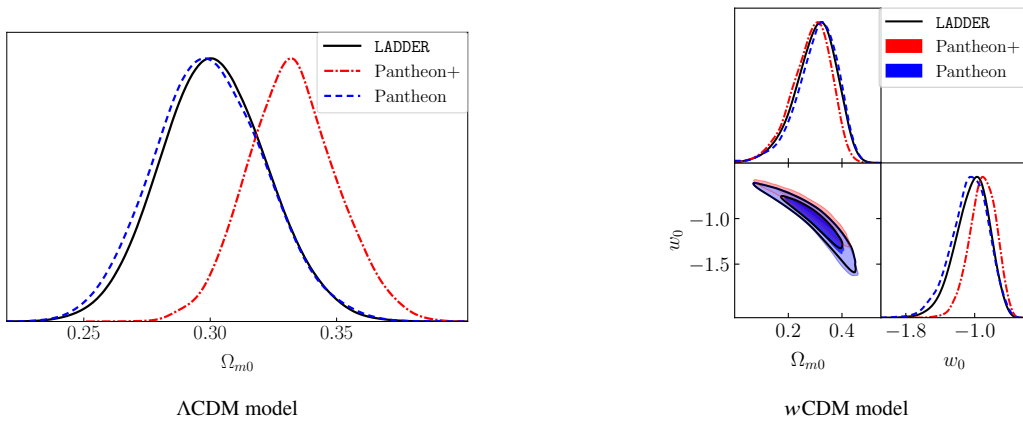


Figure 4. Cosmological parameter constraints obtained from the Pantheon and Pantheon+ datasets vs LADDER predictions.

Consistency tests, such as these, can be extended to upcoming SNIa datasets, including the recent Dark Energy Survey 5-Year Data Release announcement ([Abbott et al. 2024](#)). This dataset comprises 1829 SNIa in the redshift range of $0.10 < z < 1.13$, exhibiting a higher data density at higher redshifts compared to Pantheon+. The anticipated release of the actual data holds the

Table 2. Comparison between model parameter constraints obtained using an MCMC analysis with Pantheon and Pantheon+ dataset, vs LADDER predictions.

Datasets	Λ CDM		w CDM
	Ω_{m0}	Ω_{m0}	w_0
Pantheon	$0.299^{+0.023}_{-0.022}$	$0.316^{+0.067}_{-0.083}$	$-1.049^{+0.199}_{-0.228}$
Pantheon+	$0.332^{+0.018}_{-0.017}$	$0.292^{+0.065}_{-0.081}$	$-0.902^{+0.150}_{-0.162}$
LADDER	$0.301^{+0.021}_{-0.021}$	$0.308^{+0.069}_{-0.083}$	$-1.015^{+0.179}_{-0.216}$

potential for an exciting validation study of our ML approach. Furthermore, SNIa datasets from upcoming missions such as Euclid (Amendola et al. 2013), Rubin LSST (Zhan & Tyson 2018), Roman Space Telescope (Akeson et al. 2019), the Thirty Meter Telescope (TMT) (Skidmore et al. 2015), and the already launched James Webb Space Telescope (JWST) (Gardner et al. 2006) can serve as valuable resources for future efforts towards consistency checks.

4.2. Pathology test for different datasets in apparent tension

Since LADDER does not depend on a cosmological model, it can serve as a model-independent test for different types of data, especially those in the same redshift range as the SNIa dataset used for training. Such checks are relevant given the persistent tensions between different datasets. Here, we outline a sketch of the procedure for this with the BAO datasets. In contrast to SNIa measurements, which infer luminosity distances (d_L) from apparent magnitude values (m) by assuming an absolute magnitude (M_B), BAO measures angular distances d_A/r_d . The cosmic-distance duality relation, $d_A(z) = (1+z)^{-2}d_L(z)$, connects these quantities, with r_d being the co-moving sound horizon at the drag epoch, which needs to be calibrated for cosmological applications.

Typically, BAO measurements are combined with CMB data, which can tightly constrain r_d thereby breaking the degeneracy between r_d and d_A . In this study, we utilize BAO measurements to establish a connection between SNIa and CMB observations. We calibrate the angular distance from BAO with the LADDER predictions in a model-independent way. This enables the propagation of the CMB constraint on r_d into a constraint on M_B , or the SHOES-prior on M_B into a constraint on r_d . We attempt this exercise for two different sets of BAO data:

- Transverse Angular BAO (θ_{BAO}), comprising of 15 model-independent data points in the redshift range $0.11 \lesssim z \lesssim 2.22$, taken from the compilation in Nunes et al. (2020), obtained from SDSS-III LRGs, SDSS-IV blue galaxies and quasars.
- Anisotropic BAO (α_{BAO}), consisting of 8 Galaxy+Ly α data points in the redshift range $0.38 \lesssim z \lesssim 2.35$, from the SDSS-III, SDSS-IV DR12 and DR14 data releases, as outlined in Dialektopoulos et al. (2023).

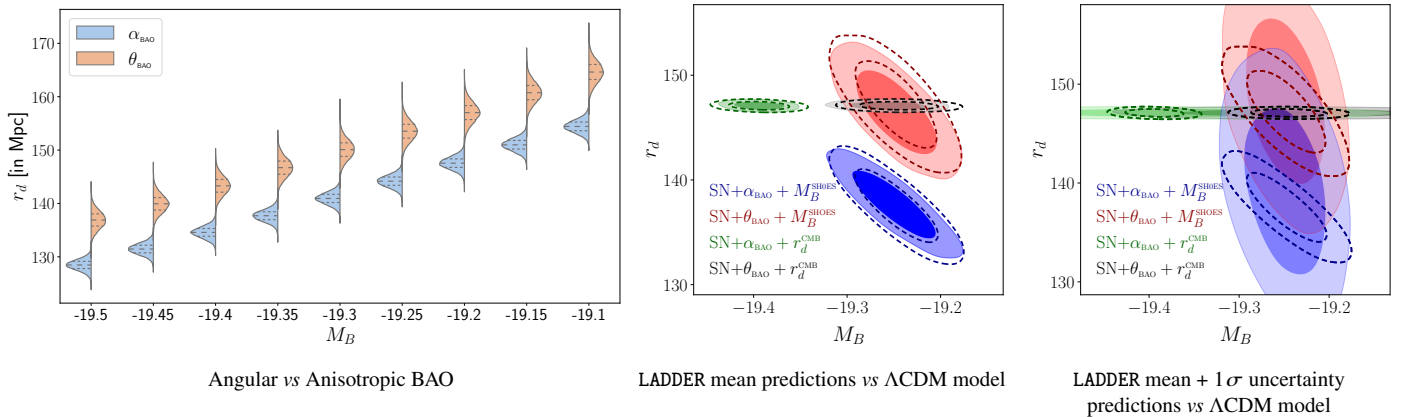
**Figure 5.** Calibration of BAO – Colored contours are LADDER predictions, dashed ones correspond to benchmark Λ CDM calibration.

Table 3. Comparison between constraints on M_B and r_d [in Mpc], employing LADDER vs vanilla Λ CDM model.

Datasets	LADDER			Λ CDM		
	M_B	r_d	H_0	Ω_{m0}	M_B	r_d
SN+ $\alpha_{\text{BAO}}+M_B^{\text{SHOES}}$	$-19.249^{+0.029}_{-0.029}$	$137.651^{+2.157}_{-2.153}$	$73.195^{+1.054}_{-1.032}$	$0.315^{+0.019}_{-0.019}$	$-19.248^{+0.030}_{-0.029}$	$137.484^{+2.312}_{-2.228}$
SN+ $\theta_{\text{BAO}}+M_B^{\text{SHOES}}$	$-19.248^{+0.028}_{-0.029}$	$146.423^{+2.697}_{-2.569}$	$73.372^{+1.023}_{-1.010}$	$0.302^{+0.022}_{-0.021}$	$-19.248^{+0.028}_{-0.029}$	$147.246^{+2.795}_{-2.712}$
SN+ $\alpha_{\text{BAO}}+r_d^{\text{CMB}}$	$-19.394^{+0.018}_{-0.017}$	$147.090^{+0.250}_{-0.267}$	$68.437^{+0.820}_{-0.826}$	$0.314^{+0.020}_{-0.019}$	$-19.394^{+0.021}_{-0.022}$	$147.087^{+0.258}_{-0.256}$
SN+ $\theta_{\text{BAO}}+r_d^{\text{CMB}}$	$-19.257^{+0.028}_{-0.027}$	$147.085^{+0.261}_{-0.253}$	$73.448^{+1.042}_{-1.025}$	$0.304^{+0.022}_{-0.021}$	$-19.245^{+0.028}_{-0.027}$	$147.088^{+0.259}_{-0.256}$

Initially, we assume different choices of $M_B \in [-19.5, -19.1]$ and constrain r_d by minimizing the χ^2 metric between the BAO data and the mean LADDER predictions at the corresponding redshifts, taking into account the full covariances associated with the BAO datasets. The direct correlation between the two calibrating parameters is evident from the monotonicity of the constraints depicted in the left-most panel of Figure 5.

However, it is noteworthy that discordant constraints on r_d exist between the two BAO datasets for a given value of M_B . This discrepancy may imply an internal inconsistency between angular and anisotropic BAO measurements, possibly attributed to the Λ CDM model dependence in anisotropic BAO data (Carter et al. 2020), an aspect that calls for further study.

We find out the difference between the vanilla Λ CDM model-dependent BAO calibration, versus our LADDER based model-independent calibration. In the middle panel of Figure 5, we show the joint constraints on the parameters M_B and r_d given different choices of priors - an astrophysical prior on $M_B^{\text{SHOES}} = -19.2478 \pm 0.0294$ (Scolnic et al. 2018) and the Planck 2018 CMB prior on $r_d^{\text{CMB}} = 147.09 \pm 0.26$ Mpc (Aghanim et al. 2020), thus breaking the degeneracy between both the parameters. Here SN refers to the Pantheon dataset. The colored contours depict LADDER mean predictions, and the dotted contours are for Λ CDM. The consistency between the two, albeit with very minor variations, suggests that the true cosmology might resemble something close to the Λ CDM model. However, the tension between angular vs anisotropic BAO measurements is apparent for both methods of calibration here, which is of considerable concern.

So, we further our pathology test by incorporating the 1σ uncertainty predictions from LADDER and redo the above exercise. Notably, the LADDER-based contours widen significantly (see right panel of Figure 5). Given uncalibrated Pantheon data, LADDER predicts a minimum as well as a maximum contour spread in comparison to the Λ CDM model. This data-driven selection of the M_B - r_d parameter space can serve as a consistency check for similar exercises with arbitrary models, to be well constrained with Pantheon SN+BAO data.

It's imperative to recall that values of M_B and r_d significantly influence H_0 (Dinda & Banerjee 2023; Chen et al. 2024; Mukherjee et al. 2024a), hence they need to be chosen with much care in the context of the prevalent Hubble tension. The contour plots in Figure 5 suggest no apparent tension between Pantheon and θ_{BAO} datasets, unlike α_{BAO} . Thus, for any cosmological analysis, the use of angular BAO data, instead of anisotropic BAO, can be recommended as long as late-time datasets are considered in conjunction. Having said that, we should leave a word of caution here. While Table 3 suggests an apparent resolution of the H_0 tension, an exhaustive Planck CMB analysis is necessary before drawing firm conclusions. Similar efforts can be undertaken with the recent Dark Energy Spectroscopic Instrument (DESI) data release serving as a valuable resource for further consistency checks between BAO data sets (Adame et al. 2024; Cortès & Liddle 2024; Colgáin et al. 2024; Wang 2024).

4.3. Model-independent calibration of high-redshift datasets

Datasets that can potentially yield d_L , but lack calibration through well-established anchors in the distance ladder, need to be calibrated by either assuming a cosmological model (Dai et al. 2004) or by some model-independent (Liang et al. 2008) means. A relevant example involves observations of GRBs which tabulate the GRB spectral peak energy E_p^{obs} and bolometric fluence S_{bolo} at different redshifts.

We investigate if LADDER, trained on uncalibrated Pantheon, can serve as a reliable model-independent calibrator for GRBs. This approach alleviates the challenge of selecting a specific cosmological model for calibration, enabling LADDER-calibrated GRBs as a unique dataset to constrain parameters across diverse cosmological models, avoiding the so-called circularity problem (Ghirlanda et al. 2006).

To demonstrate this, we use the GRB A219 sample as outlined in Liang et al. (2022) spanning the redshift range $0.03 < z \lesssim 8.2$, which correlates the spectral peak energy (E_p) and the isotropic equivalent radiated energy (E_{iso}) following Amati relation (Amati

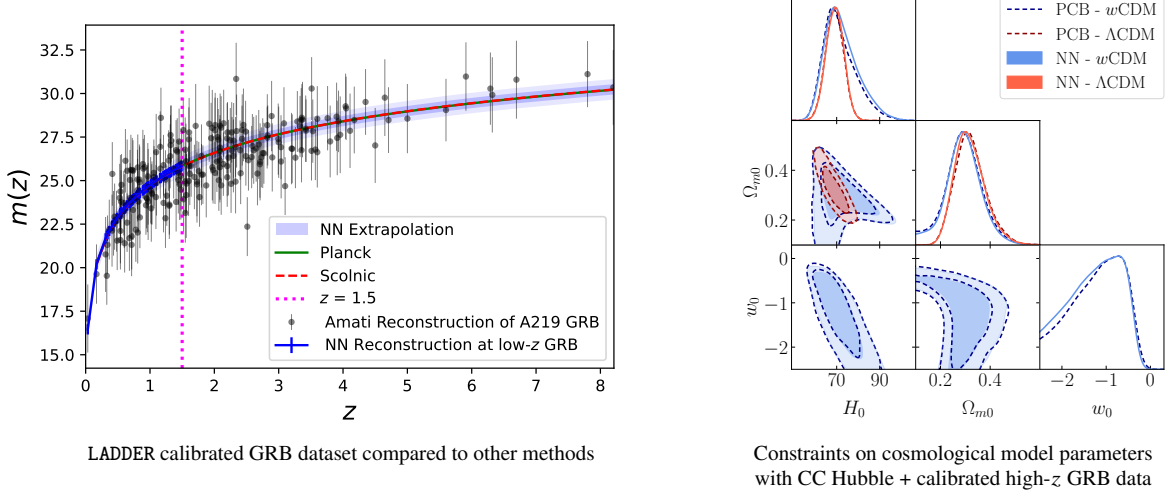


Figure 6. GRB calibration output and comparisons.

et al. 2002) as follows,

$$\log_{10} \frac{E_{\text{iso}}}{1 \text{ erg}} = a + b \log_{10} \frac{E_p}{300 \text{ keV}}. \quad (15)$$

Here, a and b are free coefficients, which connects the GRB observables to cosmic distance (Dinda 2023), such that $E_{\text{iso}} = 4\pi d_L^2(z) S_{\text{bolo}}(1+z)^{-1}$ and $E_p = E_p^{\text{obs}}(1+z)$. We then split this GRB data into low-redshift ($z < 1.5$) and high-redshift ($z > 1.5$) samples, consisting of 89 and 130 points respectively. Since LADDER predicts m directly, we express the GRB relation in terms of the same without assuming any prior values of M_B (equation (1)). To this end, the Amati relation is rewritten as, $y' = a' + b x$, where $y' = \log_{10} [(1+z)^{-1} (S_{\text{bolo}}/1 \text{ erg cm}^{-2})] + \frac{2}{5}m$. So, $a' = a + 2 \left(\frac{M_B}{5} + 5 \right) - \log_{10} [4\pi(\text{Mpc/cm})^2]$ and b are now the free coefficients to be calibrated given m vs z (Zhang et al. 2023). We use the likelihood function by Reichart (2001) to fit the parameters a' and b , using the low- z GRB sample. Table 4 shows the constraints obtained on free parameters, a' , b and the intrinsic scatter $\sigma_{\text{int}} = \sqrt{\sigma_{y', \text{int}}^2 + b^2 \sigma_{x, \text{int}}^2}$ of the Amati relation where $\sigma_{x, \text{int}}$, $\sigma_{y', \text{int}}$ are the intrinsic scatter along the x -axis and y' -axis respectively. Since LADDER has been trained to learn the distance ladder properly, we then construct a high- z GRB dataset, as shown in the left panel of Figure 6.

Table 4. Constraints on free parameters of the Amati relation - model *vis-à-vis* LADDER calibration.

	a'	b	$\sigma_{x, \text{int}}$	$\sigma_{y', \text{int}}$	σ_{int}	χ^2_{min}
LADDER	$9.915^{+0.041}_{-0.042}$	$1.599^{+0.090}_{-0.087}$	$0.157^{+0.067}_{-0.099}$	$0.274^{+0.083}_{-0.171}$	0.689	43.07
Λ CDM	$9.932^{+0.041}_{-0.041}$	$1.606^{+0.088}_{-0.086}$	$0.170^{+0.056}_{-0.109}$	$0.259^{+0.102}_{-0.169}$	0.711	47.61
w CDM	$9.924^{+0.041}_{-0.041}$	$1.605^{+0.088}_{-0.087}$	$0.164^{+0.058}_{-0.105}$	$0.258^{+0.097}_{-0.169}$	0.699	43.21

With this model-independent high- z GRB dataset we obtain constraints on parameter spaces of two cosmological models - baseline Λ CDM and the w CDM model. For the MCMC analysis, we also incorporate the 32 Cosmic Chronometer (CC) Hubble parameter measurements, as listed in Dialektopoulos et al. (2023), along with the full covariance matrix including the systematic and calibration errors (Moresco et al. 2020), covering the redshift range up to $z \lesssim 2$. The results are shown in the right panel of Figure 6. Besides LADDER, for comparison, we further calibrate the Amati coefficients employing both the above-mentioned cosmological models assuming the Pantheon SNIa + Planck2018 CMB + BAO (PCB) best-fit model parameter values. The minimized χ^2 of the Amati calibrated low- z GRB data, given in Table 4, indicates that LADDER performs slightly better than Λ CDM PCB calibration and is comparable to w CDM PCB calibration. Following this, we work out the full analysis with the respective model-calibrated datasets.

Table 5. Constraints on cosmological models with CC + calibrated high- z GRB datasets.

Model	Λ CDM		w CDM	
	LADDER	PCB	LADDER	PCB
H_0	$69.203^{+4.050}_{-4.150}$	$68.996^{+4.187}_{-4.095}$	$71.224^{+9.058}_{-6.365}$	$70.265^{+8.989}_{-5.915}$
Ω_{m0}	$0.313^{+0.066}_{-0.055}$	$0.317^{+0.067}_{-0.057}$	$0.289^{+0.068}_{-0.074}$	$0.287^{+0.072}_{-0.085}$
w_0	$-1.257^{+0.627}_{-0.867}$	$-1.172^{+0.599}_{-0.866}$

We find that the constraints obtained for Λ CDM are consistent, irrespective of the calibration method, with only a marginal widening of errors for the model-independent LADDER calibration. Similar conclusions hold when considering a beyond- Λ CDM model such as w CDM. This suggests that regardless of the cosmological model to be constrained, calibration via LADDER can provide a unique high- z GRB dataset in a model-independent setting. Further, Table 5 indicates an apparent trend towards higher H_0 values, despite not using any local H_0 prior in our analysis. While the associated uncertainties remain considerable, the observed mean shifts in H_0 are slightly more pronounced with the implementation of LADDER, compared to the outcomes obtained through model-based calibration. This disparity warrants further investigation and analysis.

GRBs are not the only challenging high-redshift datasets that need calibration independently of any cosmological model. Distance measurements involving high-redshift quasars (Dainotti et al. 2024) and early observations from the recently launched JWST (Boylan-Kolchin 2023) may also be potential candidates for the application of LADDER calibration.

4.4. Other possible applications and future directions

The persistent tension between H_0 inferred from early-time probes, assuming vanilla Λ CDM, with the directly measured H_0 from late-time observations, suggests a potential need for an alternative cosmological model. Various proposals exist in the literature (Di Valentino et al. 2021; Schöneberg et al. 2022a; Abdalla et al. 2022; Vagnozzi 2023), but none fully reconcile CMB-based model-dependent measurements with late-time direct measurements. LADDER offers the opportunity to constrain such alternative models using a broader range of datasets.

LADDER’s reasonable extrapolation feature to higher redshifts enables generation of synthetic diverse and augmented datasets. This will, in particular, be useful for cosmological forecast studies with upcoming gravitational wave missions, such as LISA (Tamanini et al. 2016), ET (Maggiore et al. 2020) and DECIGO (Mandel et al. 2018), which often requires generating mock catalogs, inherently relying on a fiducial choice of a cosmological model (Shah et al. 2023; Mukherjee et al. 2024b). We propose that our algorithm could be used as a mock data generator, based solely on the real Pantheon dataset and an assumed value of M_B .

Another major cosmological goal is the direct reconstruction of the Hubble parameter. This requires predictions on not just d_L , but also its derivatives d'_L , with associated errors. GP inherently handle this task by allowing analytical predictions of derivatives and errors, however, they struggle in data-scarce regions and completely fail where no data is available. Neural networks, despite being more performant, do not natively model d'_L and its associated error $\sigma_{d'_L}$. Although attempts to numerically differentiate the network outputs for d_L have been undertaken (Mukherjee et al. 2022; Dialektopoulos et al. 2023, 2024), these lead to substantially large uncertainties, rendering final results ineffective when it comes to precision cosmology at higher redshifts. Experiments with LADDER have shown emerging possibilities through potential applications demonstrated in the current study. We plan on expanding upon these results with further detailed analysis and hope to share our findings with the community.

5. CONCLUSION

The lack of reliable data points at high redshifts, and the smoothness of the expansion history of our Universe, makes deep learning network models prone to overfitting/underfitting issues, which significantly leads to both inaccurate and imprecise predictions. We hence propose a novel approach in using a deep learning algorithm that learns sequential data while utilizing the full covariance information among data points, applied to cosmological datasets. Our method, part of the new LADDER (Learning Algorithm for Deep Distance Estimation and Reconstruction) suite, is trained on uncalibrated SNIa data from the Pantheon compilation in a manner that is robust to outliers and noise; whilst showing appreciable precision. Our validation experiments show that LSTMs outperform other architectures and ML frameworks in performance and smoothness, perhaps suggesting the importance of capturing the sequential nature of the dataset. The resulting network also exhibits stability, even in data-sparse regions, and enables reliable predictions with associated error bars extending reliably to somewhat beyond the training data range.

Our approach shows promise for contributing to the reconstruction of the cosmic distance ladder in a model-independent manner, as opposed to the conventional cosmological model-dependent approach. We further point out to a few potential applications of LADDER, including the consistency check for similar SNIa datasets, pathology tests for other observational data in apparent tensions, and model-independent calibration of high-redshift measurements. Furthermore, our network could serve as a mock-data generator, capable of reasonable extrapolation without succumbing to overfitting. This capability opens avenues for generating model-independent, Pantheon-based data, at higher redshifts, which is crucial for forecast studies with upcoming cosmological observatories.

While we recognize other approaches, we want to gently emphasize the potential benefits of using advanced learning techniques and attempt to demonstrate how they can optimize information extraction from cosmological data. We hence wish to underscore the innovative nature of employing this new learning algorithm within the cosmological framework and extend our encouragement to the community to consider adopting this algorithm for extracting comprehensive information from cosmological data. We also reiterate that there can be some yet unexplored deep learning algorithm that may perform even better than ours. This work might encourage the community to explore them in different contexts of cosmology. Such efforts would significantly impact the accuracy and reliability of the reconstruction methods and help address yet unresolved issues of cosmology from a different perspective.

6. SOFTWARE AND THIRD PARTY DATA REPOSITORY CITATIONS

The LADDER (Learning Algorithm for Deep Distance Estimation and Reconstruction) suite and data for this article are available on [GitHub](#)² under a MIT License and version 1.0 is archived in Zenodo ([Shah et al. 2024](#)).

Software: *emcee* (Foreman-Mackey et al. 2013)

¹ We thank the anonymous reviewer for their valuable suggestions towards the improvement of the manuscript. The authors
² acknowledge the assistance received from the computational facilities made available by the Technology Innovation Hub, ISI
³ Kolkata. RS thanks ISI Kolkata for financial support through Senior Research Fellowship. PM thanks ISI Kolkata for financial
⁴ support through Research Associateship. UG and SP thank the Department of Science and Technology, Govt. of India for partial
⁵ support through Grant No. NMICPS/006/MD/2020-21. UG thanks the Indo-French Centre for the Promotion of Advanced
⁶ Research (IFCPAR/CEFIPRA) for partial support through CSRP Project No. 6702-2.

REFERENCES

- Abbott, T. M. C., et al. 2024, arXiv. <https://arxiv.org/abs/2401.02929>
- Abdalla, E., et al. 2022, JHEAp, 34, 49, doi: [10.1016/j.jheap.2022.04.002](https://doi.org/10.1016/j.jheap.2022.04.002)
- Adame, A. G., et al. 2024, arXiv. <https://arxiv.org/abs/2404.03002>
- Aghanim, N., et al. 2020, Astron. Astrophys., 641, A6, doi: [10.1051/0004-6361/201833910](https://doi.org/10.1051/0004-6361/201833910)
- Akeson, R., et al. 2019, arXiv:1902.05569, doi: [10.48550/arXiv.1902.05569](https://doi.org/10.48550/arXiv.1902.05569)
- Amati, L., et al. 2002, Astron. Astrophys., 390, 81, doi: [10.1051/0004-6361:20020722](https://doi.org/10.1051/0004-6361:20020722)
- Amendola, L., et al. 2013, Living Rev. Rel., 16, 6, doi: [10.12942/lrr-2013-6](https://doi.org/10.12942/lrr-2013-6)
- Arjona, R., Lin, H.-N., Nesseris, S., & Tang, L. 2021, Phys. Rev. D, 103, 103513, doi: [10.1103/PhysRevD.103.103513](https://doi.org/10.1103/PhysRevD.103.103513)
- Bernal, J. L., Verde, L., & Riess, A. G. 2016, JCAP, 10, 019, doi: [10.1088/1475-7516/2016/10/019](https://doi.org/10.1088/1475-7516/2016/10/019)
- Boylan-Kolchin, M. 2023, Nature Astron., 7, 731, doi: [10.1038/s41550-023-01937-7](https://doi.org/10.1038/s41550-023-01937-7)
- Camarena, D., & Marra, V. 2020, Mon. Not. Roy. Astron. Soc., 495, 2630, doi: [10.1093/mnras/staa770](https://doi.org/10.1093/mnras/staa770)
- Capozziello, S., D’Agostino, R., & Luongo, O. 2018, Mon. Not. Roy. Astron. Soc., 476, 3924, doi: [10.1093/mnras/sty422](https://doi.org/10.1093/mnras/sty422)
- Carter, P., Beutler, F., Percival, W. J., et al. 2020, Mon. Not. Roy. Astron. Soc., 494, 2076, doi: [10.1093/mnras/staa761](https://doi.org/10.1093/mnras/staa761)
- Chen, Y., Kumar, S., Ratra, B., & Xu, T. 2024, Astrophys. J. Lett., 964, L4, doi: [10.3847/2041-8213/ad2e97](https://doi.org/10.3847/2041-8213/ad2e97)
- Colgáin, E. O., Dainotti, M. G., Capozziello, S., et al. 2024, arXiv. <https://arxiv.org/abs/2404.08633>
- Cortés, M., & Liddle, A. R. 2024, arXiv. <https://arxiv.org/abs/2404.08056>
- Cuesta, A. J., Verde, L., Riess, A., & Jimenez, R. 2015, Mon. Not. Roy. Astron. Soc., 448, 3463, doi: [10.1093/mnras/stv261](https://doi.org/10.1093/mnras/stv261)
- Dai, Z. G., Liang, E. W., & Xu, D. 2004, Astrophys. J. Lett., 612, L101, doi: [10.1086/424694](https://doi.org/10.1086/424694)
- Dainotti, M. G., Bargiacchi, G., Lenart, A. L., & Capozziello, S. 2024, arXiv. <https://arxiv.org/abs/2401.11998>

² LADDER: <https://github.com/rahulshah1397/LADDER>.

- Di Valentino, E., Mena, O., Pan, S., et al. 2021, *Class. Quant. Grav.*, 38, 153001, doi: [10.1088/1361-6382/ac086d](https://doi.org/10.1088/1361-6382/ac086d)
- Dialektopoulos, K. F., Mukherjee, P., Levi Said, J., & Mifsud, J. 2023, *Eur. Phys. J. C*, 83, 956, doi: [10.1140/epjc/s10052-023-12124-3](https://doi.org/10.1140/epjc/s10052-023-12124-3)
- . 2024, *Phys. Dark Univ.*, 43, 101383, doi: [10.1016/j.dark.2023.101383](https://doi.org/10.1016/j.dark.2023.101383)
- Dinda, B. R. 2023, *Int. J. Mod. Phys. D*, 32, 2350079, doi: [10.1142/S0218271823500797](https://doi.org/10.1142/S0218271823500797)
- Dinda, B. R., & Banerjee, N. 2023, *Phys. Rev. D*, 107, 063513, doi: [10.1103/PhysRevD.107.063513](https://doi.org/10.1103/PhysRevD.107.063513)
- Escamilla-Rivera, C., Carvajal, M., Zamora, C., & Hendry, M. 2022, *JCAP*, 04, 016, doi: [10.1088/1475-7516/2022/04/016](https://doi.org/10.1088/1475-7516/2022/04/016)
- Foreman-Mackey, D., Hogg, D. W., Lang, D., & Goodman, J. 2013, *Publ. Astron. Soc. Pac.*, 125, 306, doi: [10.1086/670067](https://doi.org/10.1086/670067)
- Freedman, W. L., & Madore, B. F. 2023, arXiv. <https://arxiv.org/abs/2308.02474>
- Freedman, W. L., Madore, B. F., Hoyt, T., et al. 2020, arXiv, doi: [10.3847/1538-4357/ab7339](https://doi.org/10.3847/1538-4357/ab7339)
- Gardner, J. P., Mather, J. C., Clampin, M., et al. 2006, *Space Science Reviews*, 123, 485, doi: [10.1007/s11214-006-8315-7](https://doi.org/10.1007/s11214-006-8315-7)
- Ghirlanda, G., Ghisellini, G., & Firmani, C. 2006, *New J. Phys.*, 8, 123, doi: [10.1088/1367-2630/8/7/123](https://doi.org/10.1088/1367-2630/8/7/123)
- Giambagli, L., Fanelli, D., Risaliti, G., & Signorini, M. 2023, *Astron. Astrophys.*, 678, A13, doi: [10.1051/0004-6361/202346236](https://doi.org/10.1051/0004-6361/202346236)
- Gómez-Vargas, I., Andrade, J. B., & Vázquez, J. A. 2023a, *Phys. Rev. D*, 107, 043509, doi: [10.1103/PhysRevD.107.043509](https://doi.org/10.1103/PhysRevD.107.043509)
- Gómez-Vargas, I., Esquivel, R. M., García-Salcedo, R., & Vázquez, J. A. 2023b, *Eur. Phys. J. C*, 83, 304, doi: [10.1140/epjc/s10052-023-11435-9](https://doi.org/10.1140/epjc/s10052-023-11435-9)
- Hazra, D. K., Majumdar, S., Pal, S., Panda, S., & Sen, A. A. 2015, *Phys. Rev. D*, 91, 083005, doi: [10.1103/PhysRevD.91.083005](https://doi.org/10.1103/PhysRevD.91.083005)
- Hochreiter, S., & Schmidhuber, J. 1997, *Neural Comput.*, 9, 1735–1780, doi: [10.1162/neco.1997.9.8.1735](https://doi.org/10.1162/neco.1997.9.8.1735)
- Hornik, K., Stinchcombe, M., & White, H. 1989, *Neural Networks*, 2, 359, doi: [https://doi.org/10.1016/0893-6080\(89\)90020-8](https://doi.org/10.1016/0893-6080(89)90020-8)
- Hwang, S.-g., L'Huillier, B., Keeley, R. E., Jee, M. J., & Shafieloo, A. 2023, *JCAP*, 02, 014, doi: [10.1088/1475-7516/2023/02/014](https://doi.org/10.1088/1475-7516/2023/02/014)
- Keeley, R., Shafieloo, A., & L'Huillier, B. 2022, arXiv. <https://arxiv.org/abs/2212.07917>
- Keeley, R. E., Shafieloo, A., Zhao, G.-B., Vazquez, J. A., & Koo, H. 2021, *Astron. J.*, 161, 151, doi: [10.3847/1538-3881/abdd2a](https://doi.org/10.3847/1538-3881/abdd2a)
- Li, X., Keeley, R. E., Shafieloo, A., & Liao, K. 2024, *Astrophys. J.*, 960, 103, doi: [10.3847/1538-4357/ad0f19](https://doi.org/10.3847/1538-4357/ad0f19)
- Liang, N., Li, Z., Xie, X., & Wu, P. 2022, *Astrophys. J.*, 941, 84, doi: [10.3847/1538-4357/aca08a](https://doi.org/10.3847/1538-4357/aca08a)
- Liang, N., Xiao, W. K., Liu, Y., & Zhang, S. N. 2008, *Astrophys. J.*, 685, 354, doi: [10.1086/590903](https://doi.org/10.1086/590903)
- Liu, L., Hu, L.-J., Tang, L., & Wu, Y. 2023, *Res. Astron. Astrophys.*, 23, 125012, doi: [10.1088/1674-4527/acf6b3](https://doi.org/10.1088/1674-4527/acf6b3)
- Maggiore, M., et al. 2020, *JCAP*, 03, 050, doi: [10.1088/1475-7516/2020/03/050](https://doi.org/10.1088/1475-7516/2020/03/050)
- Mandel, I., Sesana, A., & Vecchio, A. 2018, *Class. Quant. Grav.*, 35, 054004, doi: [10.1088/1361-6382/aaa7e0](https://doi.org/10.1088/1361-6382/aaa7e0)
- Mehrabi, A. 2023, arXiv. <https://arxiv.org/abs/2301.07369>
- Moresco, M., Jimenez, R., Verde, L., Cimatti, A., & Pozzetti, L. 2020, *Astrophys. J.*, 898, 82, doi: [10.3847/1538-4357/ab9eb0](https://doi.org/10.3847/1538-4357/ab9eb0)
- Mukherjee, P., Dialektopoulos, K. F., Levi Said, J., & Mifsud, J. 2024a, arXiv. <https://arxiv.org/abs/2402.10502>
- Mukherjee, P., Levi Said, J., & Mifsud, J. 2022, *JCAP*, 12, 029, doi: [10.1088/1475-7516/2022/12/029](https://doi.org/10.1088/1475-7516/2022/12/029)
- Mukherjee, P., & Mukherjee, A. 2021, *Mon. Not. Roy. Astron. Soc.*, 504, 3938, doi: [10.1093/mnras/stab1054](https://doi.org/10.1093/mnras/stab1054)
- Mukherjee, P., Shah, R., Bhaumik, A., & Pal, S. 2024b, *Astrophys. J.*, 960, 61, doi: [10.3847/1538-4357/ad055f](https://doi.org/10.3847/1538-4357/ad055f)
- Novosyadlyj, B., Sergijenko, O., Durrer, R., & Pelykh, V. 2014, *JCAP*, 05, 030, doi: [10.1088/1475-7516/2014/05/030](https://doi.org/10.1088/1475-7516/2014/05/030)
- Nunes, R. C., Yadav, S. K., Jesus, J. F., & Bernui, A. 2020, *Mon. Not. Roy. Astron. Soc.*, 497, 2133, doi: [10.1093/mnras/staa2036](https://doi.org/10.1093/mnras/staa2036)
- Ó Colgáin, E., & Sheikh-Jabbari, M. M. 2021, *Eur. Phys. J. C*, 81, 892, doi: [10.1140/epjc/s10052-021-09708-2](https://doi.org/10.1140/epjc/s10052-021-09708-2)
- Olvera, J. d. D. R., Gómez-Vargas, I., & Vázquez, J. A. 2022, *Universe*, 8, 120, doi: [10.3390/universe8020120](https://doi.org/10.3390/universe8020120)
- Perivolaropoulos, L., & Skara, F. 2023, *Mon. Not. Roy. Astron. Soc.*, 520, 5110, doi: [10.1093/mnras/stad451](https://doi.org/10.1093/mnras/stad451)
- Reichart, D. E. 2001, *The Astrophysical Journal*, 553, 235, doi: [10.1086/320630](https://doi.org/10.1086/320630)
- Riess, A. G., & Breuval, L. 2023, arXiv. <https://arxiv.org/abs/2308.10954>
- Sanger, T., & Baljekar, P. N. 1958, *Psychological review*, 65 6, 386. <https://api.semanticscholar.org/CorpusID:12781225>
- Schöneberg, N., Franco Abellán, G., Pérez Sánchez, A., et al. 2022a, *Phys. Rept.*, 984, 1, doi: [10.1016/j.physrep.2022.07.001](https://doi.org/10.1016/j.physrep.2022.07.001)
- Schöneberg, N., Verde, L., Gil-Marín, H., & Brieden, S. 2022b, *JCAP*, 11, 039, doi: [10.1088/1475-7516/2022/11/039](https://doi.org/10.1088/1475-7516/2022/11/039)
- Scolnic, D., et al. 2022, *Astrophys. J.*, 938, 113, doi: [10.3847/1538-4357/ac8b7a](https://doi.org/10.3847/1538-4357/ac8b7a)
- Scolnic, D. M., Jones, D. O., Rest, A., et al. 2018, *Astrophys. J.*, 859, 101, doi: [10.3847/1538-4357/aab9bb](https://doi.org/10.3847/1538-4357/aab9bb)
- Shah, R., Bhaumik, A., Mukherjee, P., & Pal, S. 2023, *JCAP*, 06, 038, doi: [10.1088/1475-7516/2023/06/038](https://doi.org/10.1088/1475-7516/2023/06/038)
- Shah, R., Saha, S., Mukherjee, P., Garain, U., & Pal, S. 2024, Code: LADDER - Revisiting the Cosmic Distance Ladder with Deep Learning Approaches and Exploring its Applications, 1.0, Zenodo, doi: [10.5281/zenodo.11175054](https://doi.org/10.5281/zenodo.11175054)
- Sherwin, B. D., & White, M. 2019, *JCAP*, 02, 027, doi: [10.1088/1475-7516/2019/02/027](https://doi.org/10.1088/1475-7516/2019/02/027)

- Skidmore, W., et al. 2015, *Res. Astron. Astrophys.*, 15, 1945, doi: [10.1088/1674-4527/15/12/001](https://doi.org/10.1088/1674-4527/15/12/001)
- Tamanini, N., et al. 2016, *J. Cosmol. Astropart. Phys.*, 2016, 002, doi: [10.1088/1475-7516/2016/04/002](https://doi.org/10.1088/1475-7516/2016/04/002)
- Tang, L., Li, X., Lin, H.-N., & Liu, L. 2021, *Astrophys. J.*, 907, 121, doi: [10.3847/1538-4357/abcd92](https://doi.org/10.3847/1538-4357/abcd92)
- Vagnozzi, S. 2023, *Universe*, 9, 393, doi: [10.3390/universe9090393](https://doi.org/10.3390/universe9090393)
- Visser, M. 2005, *Gen. Rel. Grav.*, 37, 1541, doi: [10.1007/s10714-005-0134-8](https://doi.org/10.1007/s10714-005-0134-8)
- Wang, D. 2024, arXiv. <https://arxiv.org/abs/2404.13833>
- Wang, G.-J., Li, S.-Y., & Xia, J.-Q. 2020a, *Astrophys. J. Suppl.*, 249, 25, doi: [10.3847/1538-4365/aba190](https://doi.org/10.3847/1538-4365/aba190)
- Wang, G.-J., Ma, X.-J., Li, S.-Y., & Xia, J.-Q. 2020b, *Astrophys. J. Suppl.*, 246, 13, doi: [10.3847/1538-4365/ab620b](https://doi.org/10.3847/1538-4365/ab620b)
- Wei, H., Yan, X.-P., & Zhou, Y.-N. 2014, *JCAP*, 01, 045, doi: [10.1088/1475-7516/2014/01/045](https://doi.org/10.1088/1475-7516/2014/01/045)
- Xie, H., Nong, X., Zhang, B., et al. 2023, arXiv. <https://arxiv.org/abs/2307.16467>
- Zhan, H., & Tyson, J. A. 2018, *Reports on Progress in Physics*, 81, 066901, doi: [10.1088/1361-6633/aab1bd](https://doi.org/10.1088/1361-6633/aab1bd)
- Zhang, B., Xie, X., Nong, X., et al. 2023, arXiv. <https://arxiv.org/abs/2312.09440>
- Zhang, C., Bengio, S., Hardt, M., Recht, B., & Vinyals, O. 2017, in *International Conference on Learning Representations*. <https://openreview.net/forum?id=Sy8gdB9xx>
- Zhang, J.-C., Hu, Y., Jiao, K., et al. 2024, *Astrophys. J. Suppl.*, 270, 23, doi: [10.3847/1538-4365/ad0f1e](https://doi.org/10.3847/1538-4365/ad0f1e)